Agricultural and Forest Meteorology 377 (2026) 110958

Contents lists available at ScienceDirect

Agricultural and Forest Meteorology

journal homepage: www.elsevier.com/locate/agrformet

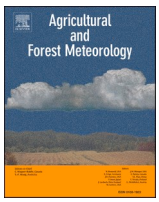

Hemispherical imaging of canopy light interception: A ceptometer alternative for precision irrigation in orchards and vineyards

Mohamed Ibrahim Belaid [a,b,*], Alexandre Escolà Agustí [b], Jaume Casadesús Brugués [a]

[a] Efficient Use of Water in Agriculture Program, Institute of AgriFood Research and Technology (IRTA), Fruitcentre, Lleida, Catalonia, Spain
[b] Research Group in AgroICT & Precision Agriculture, Universitat de Lleida/Agrotecnio-CERCA Center, Lleida, Catalonia, Spain

ARTICLE INFO

Keywords:
Crop monitoring
Canopy structure
Irrigation scheduling
Proximal sensing
Precision agriculture
Orchards

ABSTRACT

The amounts of solar radiation absorbed or intercepted by canopies are key parameters for determining gas exchange rates and for estimating water requirements and yield potential in precision agriculture. Measurements with portable ceptometers around midday are the most widespread field method for assessing light interception. However, in orchards and vineyards, light interception varies during the day depending on tree spacing, training system, and tree size, so a single midday measurement may not represent the daily integrated value. This study proposes a cost-effective approach based on hemispherical imaging for rapidly and reliably assessing both the diurnal pattern and the daily fraction of Intercepted Photosynthetically Active Radiation (fIPAR). The method uses hemispherical images representing the fraction of radiation reaching the ground across tree spacing, including alleys between rows. Images were processed automatically to analyse canopy occlusion along the sun's trajectory. Application of this method, using either still camera or video recordings, was compared with concurrent ceptometer measurements in orchard and vineyard canopies, showing high agreement (R^2 between 0.88–0.92) and consistency across lighting conditions. The results highlight that, particularly when employing action cameras, this method offers a practical, scalable, and labour-efficient assessment of diurnal fIPAR, providing an operational alternative to traditional ceptometer measurements. Its adaptability to different orchard canopies and robustness under various lighting conditions and configurations, including anti-hail nets, make it a suitable method for precision agriculture.

1. Introduction

The extent of the crop canopy is a fundamental determinant of the water requirements of most crops and particularly of fruit tree crops (Allen et al., 1998; Girona et al., 2011; Hsiao, 1990). Factors such as tree dimensions, spacing, and three-dimensional structure vary significantly between farms and are shaped by plantation design, training systems, management strategies, growth-limiting factors, and growth vigour (Scalisi et al., 2024; Tustin et al., 2022). These variations require accurate and scalable methodologies to assess tree canopy size and structure for accurate orchard management within the framework of Precision Agriculture (Sangjan and Sankaran, 2021).

Several parameters are commonly used to represent the extent of a tree canopy, including the fraction of canopy cover (fCOVER), leaf area index (LAI), and fraction of intercepted or absorbed photosynthetically active radiation (fIPAR and fAPAR, respectively) (Gower et al., 1999; Johnson and Lakso, 1991; Jonckheere et al., 2004).

Each parameter provides unique insights into the role of the tree canopy in light interception, photosynthesis, and water use. Of these, fIPAR has gained the greatest prominence on account of its ability to quantify the amount of sunlight intercepted by a canopy, which is directly linked to water requirements (Campillo et al., 2012; Green et al., 2003; Marsal et al., 2014) and crop productivity (Massonnet et al., 2008; Steduto et al., 2012; Wünsche et al., 1996). It has proven effective for modelling gas exchange, including photosynthesis and transpiration, and for predicting yield potential (Quintanilla-Albornoz et al., 2023; Scalisi et al., 2024), highlighting its central role in precision irrigation and orchard management (Lakso and Intrigliolo, 2022). Importantly, light interception directly drives transpiration, as water use in fruit trees is strongly regulated by light-sensitive stomata, particularly abundant on the abaxial leaf surface (H. Jones, 2013; Lakso, 2018).

To date, assessments of fIPAR for operational application in

* Corresponding author at: Institute of Research in Agrifood and Technology (IRTA) Fruitcentre, Parc Científic i Tecnològic Agroalimentari de Lleida (PCiTAL), Carrer de Gardeny, 4 25003 Lleida, Catalonia, Spain.
E-mail addresses: mohamed.belaid@irta.cat (M.I. Belaid), alex.escola@udl.cat (A.E. Agustí), jaume.casadesus@irta.cat (J.C. Brugués).

https://doi.org/10.1016/j.agrformet.2025.110958
Received 9 July 2025; Received in revised form 20 November 2025; Accepted 22 November 2025
Available online 24 November 2025

irrigation management are mostly based on ceptometer and light-sensors measurements (Auzmendi et al., 2011; Casadesús et al., 2011; Marsal et al., 2014). These devices are usually deployed in a predefined pattern, both above and below the vegetation (Johnson et al., 2010), and at a given moment (instantaneous fIPAR). Measurements made with ceptometers at around midday ($fIPAR_{midday}$) are assumed to provide a representative value of daily fIPAR. These measurements can be repeated at different times in the season and provide a quantitative basis for assessing the effects of pruning and/or other agricultural practices. Mobile ceptometers mounted on small vehicles have been used to measure fIPAR around midday, with measurements taken within approximately one to two hours of noon (Lampinen et al., 2012, 2014). The results can be used to compare orchards with different crop varieties and/or tree spacings, to map the spatial variability of different canopies, and to estimate the productive potential of a given orchard (,Zarate-Valdez et al., 2012, 2015a).

However, under certain orchard training systems, measurements taken at midday may not represent the entire day. Measurements should, therefore, be taken at different times and over a wide range of hours (Wünsche et al., 1995). For instance, Auzmendi et al. (2011) used a portable ceptometer to manually measure instantaneous fIPAR once every 2 h to trace the diurnal fIPAR curve.

Since taking multiple manual measurements with a portable ceptometer would be far too labour intensive for routine application, an alternative could be to continuously record instantaneous fIPAR. (Casadesús et al., 2011) used a fixed arrangement of light-sensing bars, allowing the automated adjustment of irrigation. More recently, mobile sensor systems have enabled the generation of diurnal curves of light interception with a temporal resolution of 2 h (Zhang et al., 2012), which was further refined to intervals as short as near real time resolution (Zhang et al., 2015) greatly improving the precision of whole-day fIPAR measurements. Some alternatives could include very simple approaches such as the early “chessboard” or point grid method explored in (Wünsche et al., 1995, 1996; Wünsche and Lakso, 2000), which can now be combined with modern sensor systems for automated readings.

Other innovative devices have also been developed, such as the “whirligig” (McNaughton et al., 1992), a rotating light interception system which provides highly detailed measurements of canopy light environments, well suited for scaling-up transpiration and photosynthesis measurements in apples (Green et al., 2001). Nevertheless, such setups would be too expensive for routine applications on farms, and some could also hinder the movement of machinery in the orchard (Casadesús et al., 2011).

Alternatively, the diurnal curve of fIPAR could be estimated using relatively simple models (Jackson and Palmer, 1972; Oyarzun et al., 2007; Palmer, 1977) that require measurements of tree dimensions, such as a parallelepiped. These models can be fed from UAV-based photogrammetry (Bellvert et al., 2021). However, tree shapes often depart from a perfect parallelepiped and, as a result, such measurements tend to be inaccurate.

Image analysis can provide a practical way to assess canopy properties (Lakso, 1976). Digital hemispherical photography (DHP), which involves capturing wide-angle and/or hemispherical photos looking up through the plant canopy, has been widely used for the assessment of many biophysical traits, especially in forests (Jonckheere et al., 2004; Baret et al., 2010; Fournier and Hall, 2017). Improvements in camera technology and lens capabilities have made it possible to obtain more precise images. Even so, orchards and forests represent two different types of canopies.

Common DHP processing methods typically rely on the assumption that leaves are randomly distributed within the canopy (Campbell and Norman, 1998; Jonckheere et al., 2004; Weiss et al., 2004). However, orchard canopies seldom meet this condition, as their 3D structure is highly heterogeneous and strongly influenced by pruning, training systems, and row spacing. Moreover, although DHP has been widely applied in forest studies to estimate leaf area index (LAI), in the context of orchard management, fIPAR tends to be a more straightforward parameter for irrigation purposes (Auzmendi et al., 2011).

In this context, indirect methods for estimating biophysical parameters, and particularly light interception, which rely solely on the Leaf Area Index or Leaf Area Density, such as the model presented by Campbell & Norman (1998), may not be as reliable in orchards as in forests. LAI-based estimations, which work well in forests, may underestimate fIPAR in orchards due to differences in leaf area distribution and canopy architecture.

In the context of orchard canopies, previous studies have briefly examined similar approaches based on digital photography. A comparative study of four methods for estimating light interception was conducted by Wünsche et al. (1995); this involved the use of film cameras equipped with hemispherical lenses. Campillo et al. (2008) reported a methodology for estimating light interception in a field-grown tomato crop using downward-facing photography. A similar approach was later proposed by (Zarate-Valdez, et al., 2015) but in this case was based on overhead photography of tree shadows, where the projected canopy shadow on the orchard floor was used as a proxy for intercepted radiation. However, these methods provide only a measurement of midday fIPAR rather than a daily aggregate from the diurnal curve. In addition, shadow-based approaches are strongly constrained by solar angle, weather conditions (e.g., clear skies), and the presence of uniform ground surfaces, which limits their robustness for routine monitoring.

The main objective of the present work was to analyse the performance and practical utility of an approach based on the use of hemispherical images to assess the diurnal curve of fIPAR in tree crops and vines. The method consists of (1) taking samples in the tree spacing between rows of trees, using photos or videos, to obtain a mosaic of upward-facing hemispherical images of the canopy; (2) analysing the images by an automated software that overlays the calculated diurnal solar trajectory on the segmented canopy of each image and; (3) aggregating data to obtain a diurnal fIPAR curve for the whole tree spacing, including one-half of the trees on either side of the alleyway and the alleyway itself. The still camera setup, with stable mounting and controlled position would allow for consistent image acquisition. In contrast, video recording with an action camera held on a selfie stick would allow a faster and lower effort image acquisition.. The performance of both approaches was then evaluated by comparing their outputs to measurements obtained through a standard ceptometer method.

2. Materials and methods

2.1. Methodological workflow

2.1.1. Procedure for image acquisition

For both fixed camera pictures and action camera videos, the procedure consisted of recording a collection of hemispherical upwards-looking images of the canopy, following a pre-defined pattern, recording the area between two adjacent rows of trees The camera was placed near the ground and levelled to achieve a zenith view, with vertical axis of the images aligned parallel to the tree rows (see Fig. 1).

2.1.2. Still camera with self-levelling platform

A D70 (Nikon, Tokyo Japan) reflex camera equipped with an AT-X 107 DX (Tokina, Tokyo, Japan) fisheye zoom lens was mounted on a custom-made self-levelling support, which maintained the camera in an upward zenithal view, regardless of the ground slope. The lens height was about 20 cm above the ground. The support, which had a base footprint of 50 cm x 50 cm, was manually moved to different positions following a chessboard sampling pattern (Fig. 1). Photos were taken within the alleyway, at 100 cm intervals, covering the full distance between rows.

2.1.3. Action camera

A HERO10 Black (GoPro, California, USA) action camera was

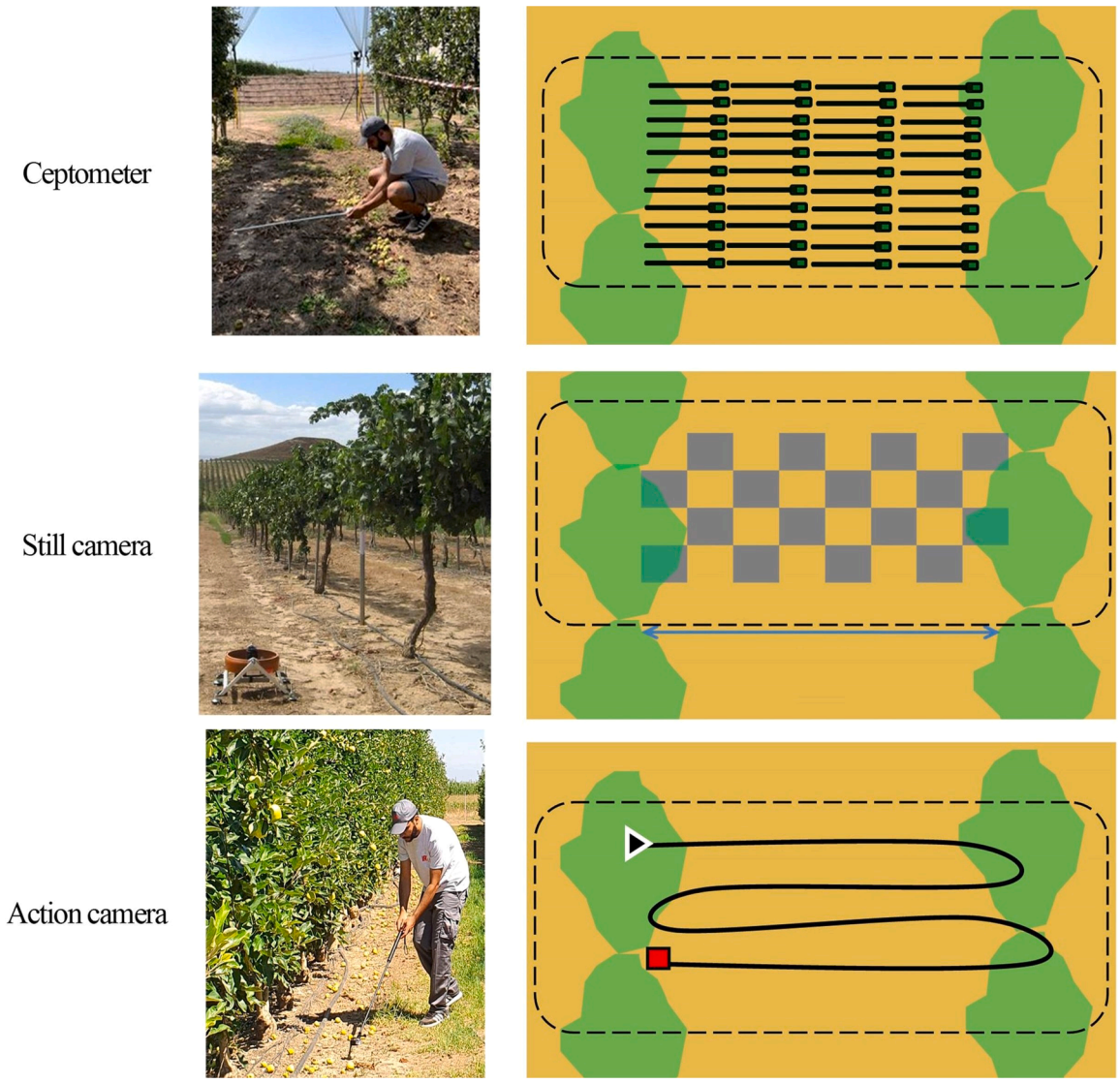

Fig. 1. fIPAR sensing devices employed (left column) with their corresponding sampling patterns (right column) and interrow sampling area (dashed).

mounted on a selfie stick for mobile image acquisition. Sampling involved recording videos with the camera held upwards and at approximately 20 cm from the ground, while following an on-the-go zigzag pattern between two rows of trees that included at least three consecutive trees in each row (Fig. 1). Efforts were made to keep the camera levelled and well-oriented and to move at a constant speed between the trees during video recording to ensure uniform sampling. The video footage was subsequently divided into individual frames (at a rate of 1 frame per second), which were treated similarly to the still photograph images.

2.1.4. Image analysis

Custom-made software was developed in Python for processing the images, using version 1.6 of the OpenCV library (Bradski, 2000). In the case of the video images recorded with the action camera, the first step in the processing workflow involved extracting individual frames from the video footage. One frame per second was selected for image extraction, from the initial 60 frames per second of video footage.

Each image was a sample of the canopy, from a distinct position in the tree spacing. The sky background visible in each image represents the canopy gaps from that position within the tree spacing. Overlaying the sun path onto the image reveals the fraction of sunlight intercepted by the canopy at different times of the day. The complete set of images provides a representative sampling of canopy light interception across the entire tree spacing.

The fIPAR curves corresponding to the different images in the sampling pattern were then integrated to create a single diurnal curve for the whole canopy. The whole processing described below was automated with this software. Usage of the software involved selecting the folder containign the images, selecting the camera -whose properties had previously been configured- and specifying longitude, latitude and row orientation. The typical processing of a canopy involved few seconds in a normal desktop computer.

2.1.5. Canopy segmentation from the sky background

Following the approach of (Casadesús et al., 2007) in each image, the pixels corresponding to the canopy were separated from the background using thresholds based on a converted HSV (Hue, Saturation, Value) colour space.

The pixels considered to correspond to the canopy ($canopy_{mask}$) were determined by removing those matching the colour of a blue sky ($blue_{mask}$) and those matching the colour of a cloud or an overcast sky ($lightgrey_{mask}$) from the initial image.

$$canopy_{mask} = whole\_image - -(blue_{mask} - - lightgrey_{mask}) \quad (1)$$

Where: $canopy_{mask}$ includes all the pixels considered to correspond

to part of the canopy; the whole_image is the total set of pixels in the image; the $blue_{mask}$ includes all the pixels whose hue values fall within a range of different blue sky tones, from hue_{min} to hue_{max}, which in this work corresponded to values of 180 and 270, respectively, on a scale from 0 to 360; $lightgrey_{mask}$ includes all the pixels whose combination of saturation and intensity falls within the range typically associated with cloud brightness. This was parametrized as saturation lower than sat_{max}, and intensity greater than $intensity_{min}$, which in this work corresponded to $sat_{max} = 20$, and $intensity_{min} = 60$, on a scale from 0 to 100. These threshold values were empirically optimized through iterative testing on representative image samples.

During the process of taking photographs and recording video during daylight, the presence of the sun disk in the scene can produce regions where the colour values of the affected pixels are overflown and, hence, undetermined (Fig. 2). These regions are referred to as *sun flares* (Kotp and Torki, 2023, 2024). Further details on their characteristics and detection methods can be found in these references. Pixels of these regions are considered background (sky), which is true in most cases. However, part of the actual canopy pixels neighbouring those regions can be flared as well and then, eroded from the canopy region and erroneously accounted as background.

The maximum impact of this issue was quantified as the percentage of flared pixels in the sampled images.

Broad application of the method to different horticultural scenarios, must consider the possibility of using anti-hail nets. In that case, support structures of various colours, including poles and bars, may appear in the background when upward-facing images are taken. Tests of the method were conducted under hail nets with different properties to determine whether the thresholds should be specifically adapted to the properties of each anti-hail net.

2.1.6. Projection of the diurnal path of the sun on the images

On each image, a curve was traced by the designed software, representing the position of the sun at different times in the day. This was based on the field of view of the cameras and the traced path of the sun in x and y pixel coordinates. It was calculated using the geographical coordinates of the orchard, the day of the year, the camera azimuth and the optical calibration of a hemispherical lens camera. Firstly, the elevation of the sun and its azimuth were calculated for each hour of the day, based on (Allen et al., 1998). Fig. 3 illustrates the two angles involved, from Masters (2004).

Based on the latitude (φ), longitude (L) and corresponding day of the year (DOY), the solar curve parameters are:

Fig. 2. Example of some of the challenges to canopy analysis posed by background factors, such as different coloured anti-hail nets and pixels affected by sun flares.

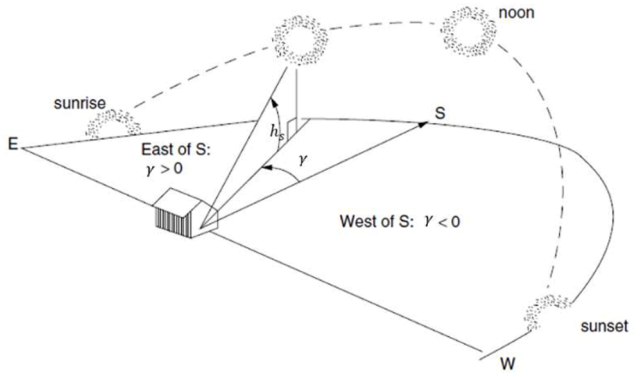

Fig. 3. Sun curve parameters (angle of the azimuth γ and elevation h_s), from Masters (2004).

$$\text{Declination of thr sun (Radians)},\ \delta = 0.409\sin\left(\frac{2\pi}{365 * DOY} - 1.39\right) \tag{2}$$

$$\text{Elevation of the sun (Radians)},\ h_s = \sin^{-1}(\sin\varphi\sin\delta + \cos\omega\cos\delta) \tag{3}$$

$$\text{Sun azimuth angle (Radians)},\ \gamma = \tan^{-1}\left(\frac{-\cos\delta\cos\varphi\sin\omega}{\sin\delta - \sin\varphi\sin h}\right) \tag{4}$$

$$\text{Solar time angle (Radians)},\ \omega = \frac{\pi}{12}[(t + 0.06667(L_z - L_m) + S_c) - 12] \tag{5}$$

$$S_c = 0.1645\sin(2b) - 0.1255\cos(b) - 0.025\sin(b) \tag{5.1}$$

Where: S_c is a seasonal correction for solar time in hours, t is the standard clock time in hours, L_z is the longitude of the centre of the local time zone in degrees, L_m is the longitude of the measurement site in degrees (Allen et al., 1998).

Secondly, the apparent path of the sun in the sky, represented by its hourly elevation and azimuth, was converted into a curve in the image and represented by a list of pixel coordinates.

Given the height (h) and the width (w) of the image, the elevation of the sun (h_s) and its azimuth (γ_s), the azimuth of the camera (γ_c) and calibrated conversion from pixel coordinates to corresponding camera and lens angles (α_c), the coordinates (x, y) of the position of the sun in the image were computed automatically following Eq. (6).

$$\begin{pmatrix} x \\ y \end{pmatrix} = \begin{pmatrix} \frac{w}{2} - x_i \\ \frac{h}{2} - y_i \end{pmatrix} \tag{6}$$

Where:

$$\begin{pmatrix} x_i \\ y_i \end{pmatrix} = \begin{pmatrix} r\sin(\gamma_s - \gamma_c) \\ r\cos(\gamma_s - \gamma_c) \end{pmatrix} \tag{6.1}$$

$$r = \alpha_c\cos h_s \tag{6.2}$$

2.1.7. Determination of the diurnal fIPAR curve

The procedure assumed that fIPAR at a given time of day consists of two components. The beam component depends on the fraction of canopy pixels located in the part of the image where the sun is expected to appear at that specific time. The diffuse component depends on the overall fraction of canopy pixels across the entire image. In each individual image, computation was made by defining a series of rectangles that followed the path of the sun. Each of these represented the position of the sun at a given time of day.

Two variables were calculated for each rectangle. Firstly, the beam fIPAR ($fIPAR_{beam}$), which was dimensionless, determined as the fraction of canopy pixels compared to the total number of pixels in the rectangle. Secondly, the quantity of potentially intercepted PAR at a given time, $PIR_{instantaneous}$, on a clear day, was determined as shown in Eq. (7):

$$PIR_{instantaneous} = fIPAR_{beam} * R_S * (1 - K_d) + fIPAR_{img}\ R_S * K_d \tag{7}$$

Where R_S is the expected solar radiation under a clear sky at the location in question, on the day of the year and at the chosen time of day, $fIPAR_{img}$ is the fraction of canopy pixels for the total image, and K_d is a coefficient that represents the fraction of diffuse radiation. The role of R_S and K_d in (Eq.7) is to bring a weight to each point in the diurnal curve related with the expected solar radiation at that time of the day.

The source for R_S and K_d depends on the intended application of fIPAR assessment. For irrigation management purposes, these values should represent the typical radiative conditions of a clear day for that region and season, rather than the actual measurements for a given day.

For that, the radiation regime chosen was that of clear sky, based on the theoretical beam radiation proposed in (Allen et al., 1998):

$$R_S = 0.75\ R_a \tag{8}$$

$$R_a = \frac{60}{\pi}\ Gs * \ dr\ (\omega_2 - \omega_1)\sin\varphi\sin\delta\cos\varphi\cos\delta(\sin\omega_2 - \sin\omega_1) \tag{8.1}$$

$$d_r = 1 + 0.033\cos\left(\frac{2\pi}{365}n\right) \tag{8.2}$$

Where: R_a, in W/m^2 is the extraterrestrial radiation; Gs is the solar constant (1366 W/m^2); d_r (dimensionless) is the inverse relative distance between the Earth and the Sun; φ and δ, expressed in radians, are the latitude and the declination of the sun; ω_1 and ω_2 are the solar time angles at the beginning and at the end of the period, expressed in radians.

To account for the diffuse component of radiation when assessing the diurnal fIPAR, the fraction of diffuse radiation, K_d, was assumed to be equal to 0.2 to represent typical clear-sky conditions, providing a standardized basis for comparison across sites and dates. In practice, K_d can vary considerably depending on atmospheric conditions and solar elevation, yet it is rarely measured directly. Using a constant value therefore avoids introducing unnecessary variability into the fIPAR estimates and ensures that comparisons between canopies from different orchards or periods, reflect structural differences rather than transient meteorological effects.

To allow visual inspection of the process, the software saved a processed copy of each image, in which the rectangles and the diurnal curves of $fIPAR_{beam}$ and $PIR_{instantaneous}$ were overlapped (Fig. 4). As commented above, the presence of sun flares in the scene may result in an underestimation of the number of canopy pixels. To compensate this effect, a second series of rectangles was added, which rarely contained sun flares. This symmetry corresponds to the pattern observed in the first series of projected rectangles, assuming that canopy properties are similar on both sides of the East–West axis.

2.1.8. Converting diurnal curves to a daily fIPAR value

For hands-on application, in many situations, using a single daily value that summarizes the diurnal fIPAR curve could be more practical than using the curve itself (Drechsler et al., 2022; R. S. Johnson et al., 2000). This value was calculated as shown in Eq. (9).

After determining the diurnal curves of $fIPAR_{beam}$ and $PIR_{instantaneous}$ for all the individual images of a given canopy, the completed curves for the whole tree spacing are obtained by averaging the corresponding diurnal fIPAR curves across images. All these calculations were carried out automatically using the algorithm that was developed. In practice, it was a weighted average of the instantaneous fIPAR, where the weights were provided by the R_s values at that time.

$$fIPAR_{daily} = \frac{\sum PIR_{instantaneous}}{\sum R_s} \tag{9}$$

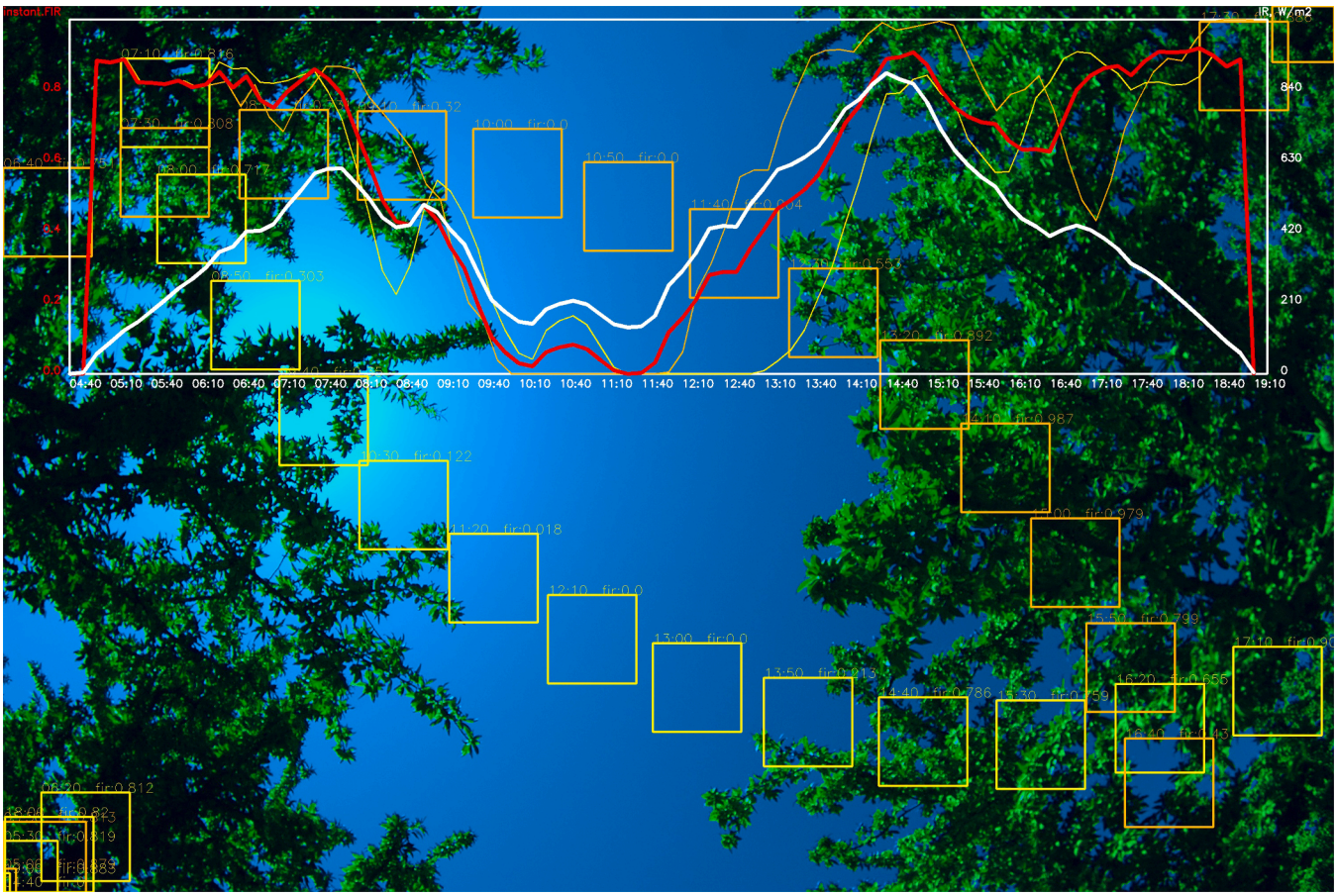

Fig. 4. Example of a diurnal curve of fIPAR obtained from a photo taken using a still camera on an almond orchard with tree rows oriented 30º North. It shows: Yellow rectangles: defined area analysed that followed the path of the sun; Orange rectangles: a mirror image of the area of analysis; Yellow line: the $fIPAR_{beam}$ for the area analysed; Orange line: the $fIPAR_{beam}$ for the mirror image of the area analysed; Red line: the average $fIPAR_{beam}$; and white line: $PIR_{instantaneous}$ (W/m^2).

2.1.9. Camera calibration

Camera calibration consisted of establishing how each pixel in the image corresponds to a specific observation angle. This relationship depends on the camera and lens used and is essential to accurately project the sun's path onto the images. The dataset for calibrating each camera was obtained by sampling a known pattern. This was carried out in lab, using the same lens and camera combination options that were used in the field. Both the still camera and the action camera were firmly mounted on tripods, aimed at a board marked with magnets positioned

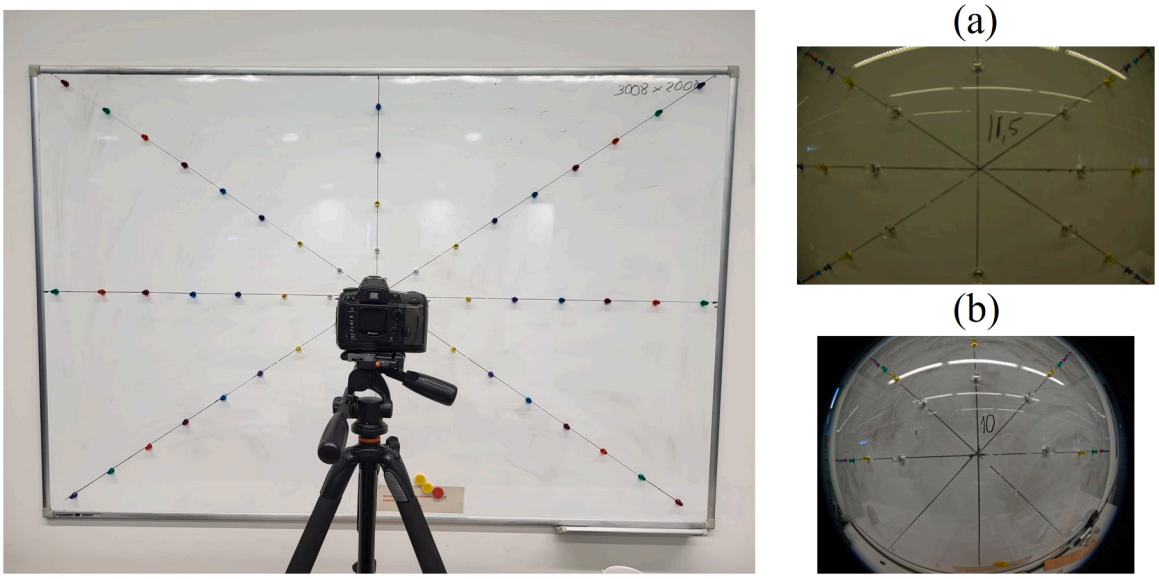

Fig. 5. Board configuration for camera calibration (left). Example of images taken by the still camera (a) and by the action camera (b).

at precise, known coordinates (Fig. 5).

Similarly to Díaz et al. (2024), this setup allowed us to calibrate the cameras by correlating the observation angles of the magnets with their coordinates in the recorded images. (Fig. 6).

Magnets were organised on the board in a star configuration. Having magnets of different colours facilitated the task of identifying them in the images and referring to their positions on the board. (Fig. 2). Photographs and short videos were obtained with three different distances between the board and the cameras to allow a varied range of angles.

For each picture or video frame, the viewing angle for each magnet was calculated as follows:

$$\text{Angle} = \arctan\left(\left(\frac{d_{magnet,\ center}}{d_{\ camera,board}}\right)\right) \quad (9a)$$

Where: $d_{magnet,\ center}$ is the distance in cm between the magnet and the centre of the board.

$d_{camera,\ board}$ is the distance in cm between the camera and the board.

The parameter to be calibrated was the slope of the relationship between the distance in pixels from each magnet to the centre of the image and the viewing angle for each magnet (projection function of the camera). The combination of cameras, lenses and settings produced different fields of view in the sampled images (Table 1).

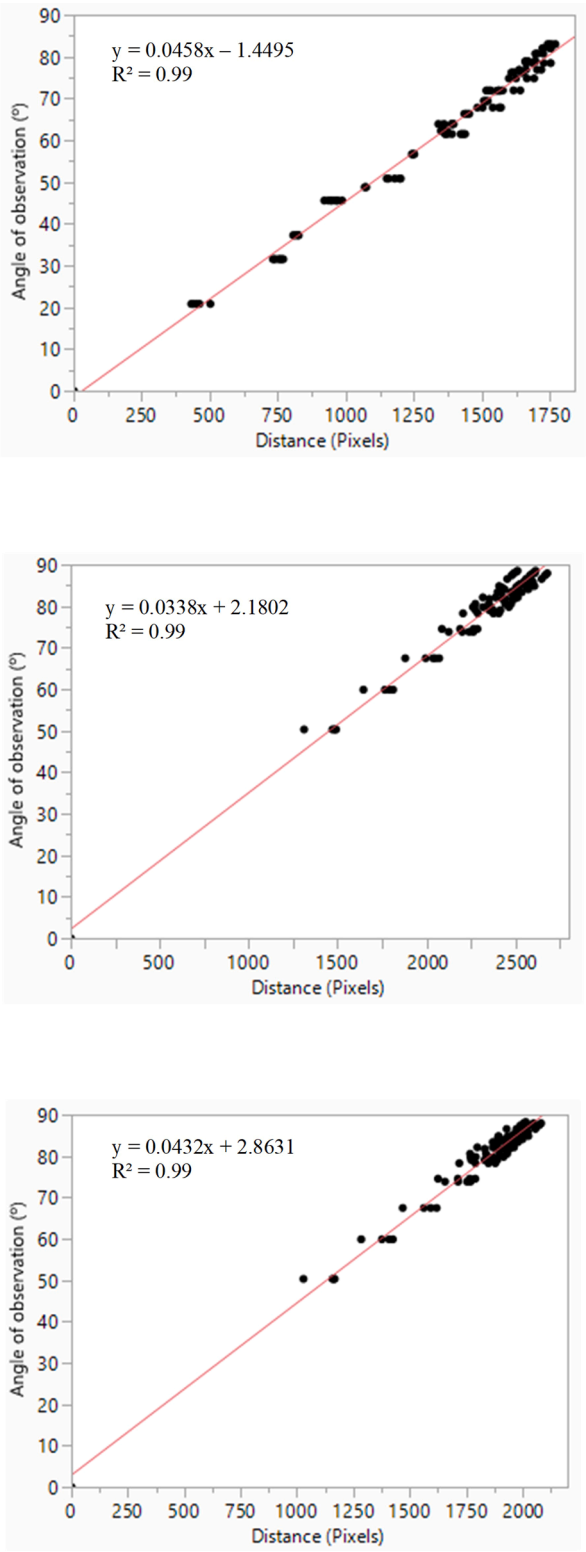

Fig. 6. Correlations between the angle of observation (in degrees) and the distance ($d_{magnet\text{-}center}$) (in pixels) for the still camera (a) and action camera in SuperView mode (b) and WideAngle mode (c).

2.2. Datasets

To validate the DHP methodology, two datasets were created and used. The first: Dataset 1, was obtained from a large and spatially heterogeneous vineyard located at Raimat, Lleida, Spain, where the canopies of four sites were analysed. These involved two grape varieties at two topographic locations, resulting in different vine development patterns: *Vitis vinifera* cv. Chardonnay-large, *Vitis vinifera* cv. Chardonnay-small, *Vitis vinifera* cv. Pinot-large and *Vitis vinifera* cv. Pinot-small. fIPAR was sampled using a still camera under two different light conditions, corresponding to consecutive days: dawn, with overcast sky, and during the day with a cloudless sky. This was done to evaluate the consistency between the two sampling conditions. On the second day, instantaneous fIPAR was also measured, using a ceptometer (AccuPAR model LP-80; Decagon Devices Inc., Pullman, WA, USA), at 2-hour intervals, from sunrise to sunset.

The second dataset: Dataset 2, was designed to compare the labour effort and accuracy of the fIPAR measurements obtained with each approach. To do this, hemispherical photographs were obtained with a still camera and hemispherical video footage was recorded with an action camera. Images were obtained in an apple orchard, a vineyard and an almond orchard (Fig. 7). At each site, data were collected over three consecutive clear-sky days (3 repetitions): Mollerusa (April 17–19), Raimat (May 29–31), and Les Borges Blanques (July 15–17). The datasets are summarized in Table 2. Another extensive dataset, relating to the same apple orchard that was used for the second dataset, was also acquired. This included fisheye images featuring canopies of various dimensions (large and small) and different backgrounds (with clear and overcast skies and anti-hail nets of different colours) to examine the influence that the background had on the assessment.

For the measurements made by a portable Ceptometer (AccuPAR model LP-80; Decagon Devices Inc., Pullman, WA, USA), readings were taken in the tree spacing, between the rows of trees; below the canopy, at different positions in the alleyway (Fig. 1).

Ceptometer readings were collected under clear sky conditions to minimize short-term fluctuations in incident radiation. At each sampling location, 30 consecutive readings were recorded and averaged to reduce random variability. The ceptometer was positioned consistently at a fixed height below the canopy and aligned perpendicular to the row direction to ensure a uniform sampling geometry. These procedures limited measurement errors related to operator handling, solar zenith angle, and sky transience. Readings were taken at 0.5 m intervals (PAR_{below}), after recording the incident PAR (PAR_{total}). Instantaneous fIPAR was then calculated as follows:

$$fIPAR_i = 1 - \sum_{i=1}^{N} \frac{PARi_{below}}{PAR_{total}} \quad (10)$$

Table 1
Still and action camera configurations and FOV analysis.

Camera	Lens model	Settings	Picture frames (height x width pixels)	Diagonal fov (degrees)	Horizontal fov (degrees)	Vertical fov (degrees)	Calibrated degrees/pixel
Still camera (Nikon d70)	Tokina Fisheye	Widest zoom, infinity focus	3008×2000	165	138	92	0.0458
Action camera (Gopro Hero 10)	Action Camera Max Lens	"SuperView" Mode	5568×4176	>180	>180	141	0.0338
		"WideAngle" Mode	4000×3000	>180	173	130	0.0432

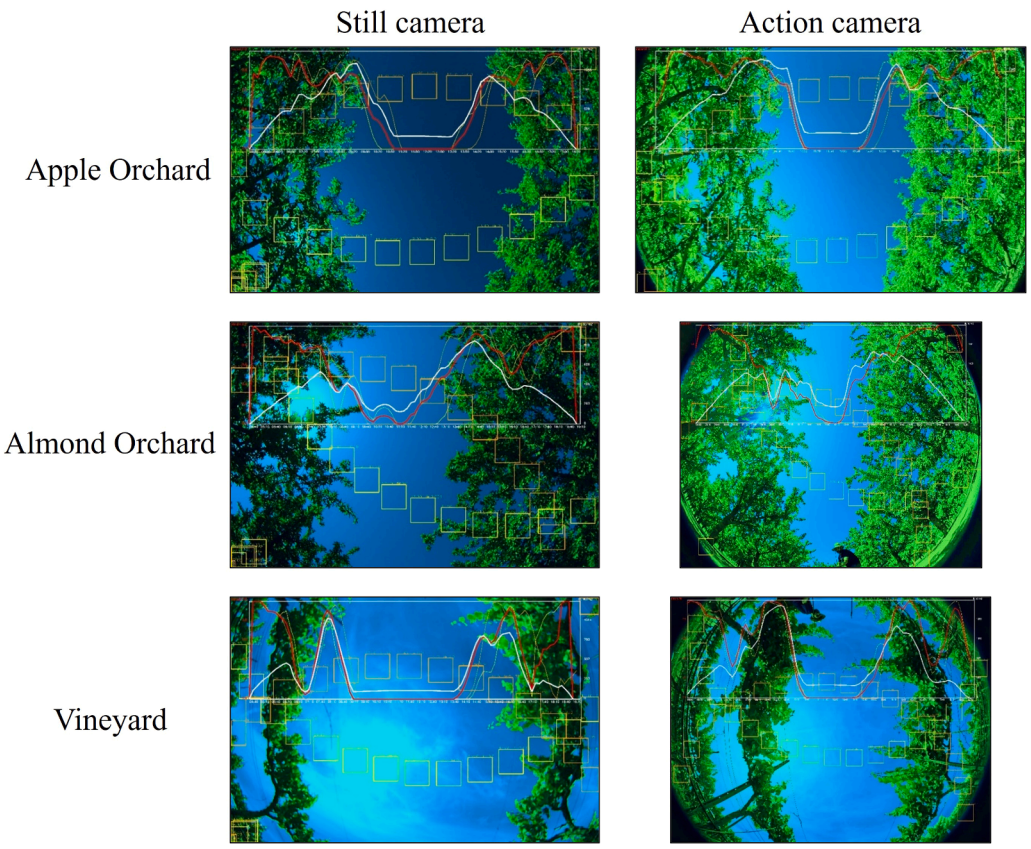

Fig. 7. Sample images from a still camera (photographs) and an action camera (video frames) showing different canopies. In the action camera image, the video mode was set to Wide Angle for apple trees but to SuperView for almond trees and vineyards.

Where N is the number of readings taken, both in the alleyway and below the trees.

2.3. Statistical analyses

JMP statistical software v17.2.0 (SAS Institute Inc., Cary, USA) was used in the analysis. It was particularly used to examine the relationship between the diurnal curves derived from photographs and to check how they corresponded to the ceptometer readings. The coefficient of determination (R^2) was computed to quantify the strength of the relationships.

3. Results

The accurate assessment of diurnal and daily fIPAR based on sampled photos and frames required careful preprocessing. This began with camera calibration and checking the FOV of still and action cameras and ensuring that conversion was possible. This was followed by an evaluation of the canopy segmentation performance, which determined how effectively the plant and non-plant areas could be distinguished. Once the segmentation had been validated, the ability of the algorithm to capture diurnal fIPAR curves was assessed. Diurnal curves were computed for each photo and/or video frame. The process consisted of analysing a series of instantaneous fIPAR values, which had been calculated at 10-minute intervals throughout the day. To further refine the approach, a comparison was made between the images obtained using still and action cameras.

3.1. Camera calibration

The calibration results indicated a field of view of 165° for the still camera along the diagonal, with narrower angles in the middle of the horizontal and vertical axes (Table 1). The field of view of the action camera was notably wider (180°), in both the video and photo modes, which made it possible to capture a broader range of the diurnal curve. The action camera had different fields of view for its photo and video modes (Table 1). The video mode exhibited a slightly narrower diagonal FOV compared to the photo mode, though both were wider than that of the fisheye lens on the still camera. Despite this difference, the video mode was more practical for field applications due to its capacity to record continuously, this simplified data collection in the field. This continuous capture reduced the time spent repositioning the camera and

Table 2
Summary of orchard characteristics, sampling conditions, and data collection parameters for the different datasets.

Dataset	1	2		
Orchard	**Vineyard (*Vitis vinefera*)**	**Apples (*Malus domestica*)**	**Vineyard (*Vitis vinefera*)**	**Almonds (*Prunus dulcis*)**
cv.	Chardonnay (Large, small); Pinot (Large, small)	Golden Reinders	Chardonnay	Vairo
Rootstock	1103 Paulsen	M9	1103 Paulsen	INRA GF-677
Training system	Trellis	Bi-axis Spindle	Trellis	Open Vase
Orchard age (Years)	>10	>10	>10	>10
Cover Crop	No	No	Yes	No
Location (ETRS89 coordinates)	Raimat (41° 40′ N–0° 28′ E)	Mollerusa (41° 63′ N–0° 9′ E)	Raimat (41° 40′ N–0° 28′ E)	Les Borges Blanques (41° 30′ N–0° 51′ E)
Tree spacing	Chardonnay: 2 m x 3 m. Pinot: 1.7 m × 3 m	1.2 m × 3.6 m	1.7 m × 2.5 m	3.5 m × 5.5 m
Row orientation	12° east	4° west	6° east	30° east
Tree dimensions (height, width, depth)	Chardonnay Large: 2 m × 1 m × 0.5 m. Chardonnay Small: 2 m × 0.7 m × 0.3 m Pinot Large: 1.7 m × 1.2 m × 0.7 m. Pinot Small: 1.7 m × 0.6 m × 0.3 m	3.2 m × 1.2 m × 0.6 m	1.7 m × 0.7 m × 0.5 m	3.5 m × 2.5 m × 1.3 m
Sampling DOY	203–204	108–109–110	150–151–152	199–200–201
Cloudiness	DOY 203 overcast at dawn; DOY 204 cloudless	Cloudless	Cloudless	Cloudless
Num photos/sampling	30	30–35	25–30	40–45
Seconds video/sampling	-	30–40	30–40	50–60
Cept measur. /Sampling	60 in the alley + 6 reference	30 in the alley + 5 reference		
Sampled trees	6	6	6	6

made it possible to carry out a faster sampling.

3.2. Canopy segmentation in individual images

The approach previously described required segmentation of the images to distinguish between the canopy and background. Overall, the classification of the pixels based on colour space Intensity-Hue-Saturation (I, H, S) make it easy to distinguish the foreground from the sky background. The sky typically ranges from blue under clear conditions to various shades of grey, depending on cloud cover.

Visual examination showed that in some of the images taken during daylight, sun flares appeared as bright white areas, due to overexposure, which the algorithm classified as background, since their color matches that of clouds. However, some of these overexposed pixels may correspond to leaves at the canopy border, which appear eroded by the sun flare and would be misclassified as background (Fig. 2). Sun flares did not occur in images obtained at dawn, in which the distinction between the canopy and the background was much clearer. The erosion at the canopy border by sun flares was less evident for larger canopies, possibly because denser canopies prevented it.

One estimate of the potential maximum error introduced by sun flares was derived by quantifying the proportion of bright white pixels associated with sun flares relative to the total number of pixels analyzed by the algorithm in each image, which also yielded a value below 3 % (Fig. 8). The actual error is expected to be lower than this estimate, since part of the bright white pixels are correctly classified as background.

The background thresholding process was based on certain ranges of H, S, and I, and the results obtained indicated that its parameterization could be applied across a wide range of background conditions, including blue skies, skies with different degrees of cloud cover, and even images that included the presence of greyish anti-hail nets. However, in the case of coloured anti-hail nets, which were yellow in this case, it was necessary to slightly modify the thresholding technique as the algorithm mistakenly classified smaller parts of them, specially shaded areas, as within the acceptable colour range for the canopy (Fig. 9). In the images analysed, the canopies were viewed from below. The images obtained were mostly composed of leaves, stems, and growing fruits, while parts of the trellis system, such as poles and wires,

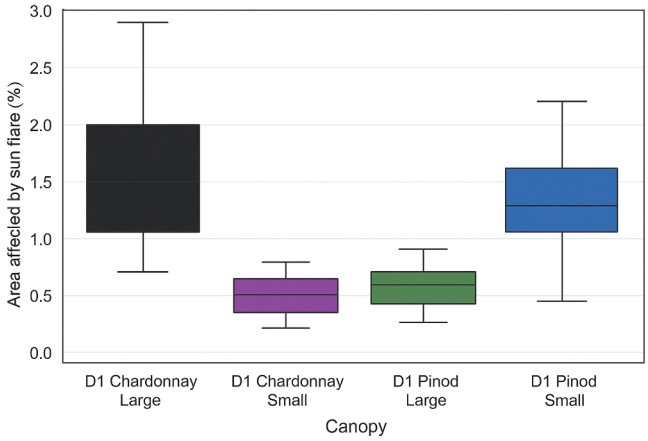

Fig. 8. Maximum potential error caused by sun flares, estimated for each image as the proportion of bright white pixels associated with sun flares relative to the total number of pixels analyzed by the algorithm.

also appeared in the foreground. For the purposes of this study, all these objects were considered as part of the canopy.

3.3. Validation of the diurnal pattern of light interception

Diurnal fIPAR curves were measured with the proposed method for four vineyard canopies using the still camera. The results were then compared to ceptometer readings collected throughout the daylight hours. Each of the canopies analysed in this study showed a different, and distinct, diurnal pattern of fIPAR. These patterns could be clearly discerned by applying both the hemispherical imaging approach and using ceptometers.

Overall, the continuous diurnal patterns of fIPAR obtained using hemispherical imaging tended to match the discrete measurements recorded by ceptometers at different times of the day. R^2 values of 0.88 and 0.92, with mean square differences of 0.07 and 0.08, were respectively obtained for hemispherical imaging sampled at daytime and dawn

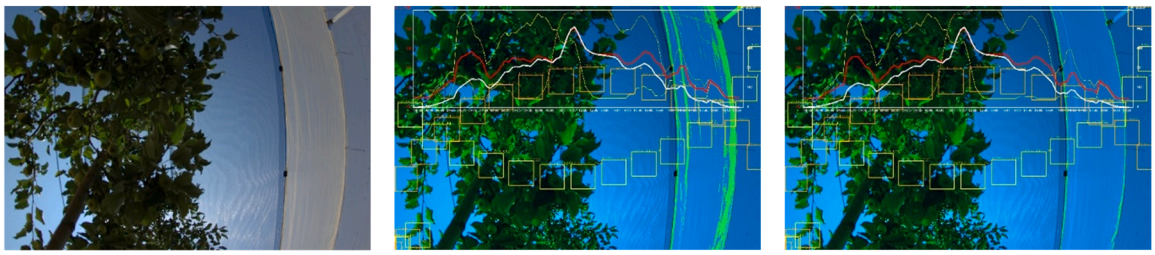

Fig. 9. Correction of thresholding process for yellow anti-hail nets: (a) original image with anti-hail net interference, (b) initial segmented image with the anti-hail net misclassified as part of the canopy, and (c) corrected image, after adjustment of thresholding process.

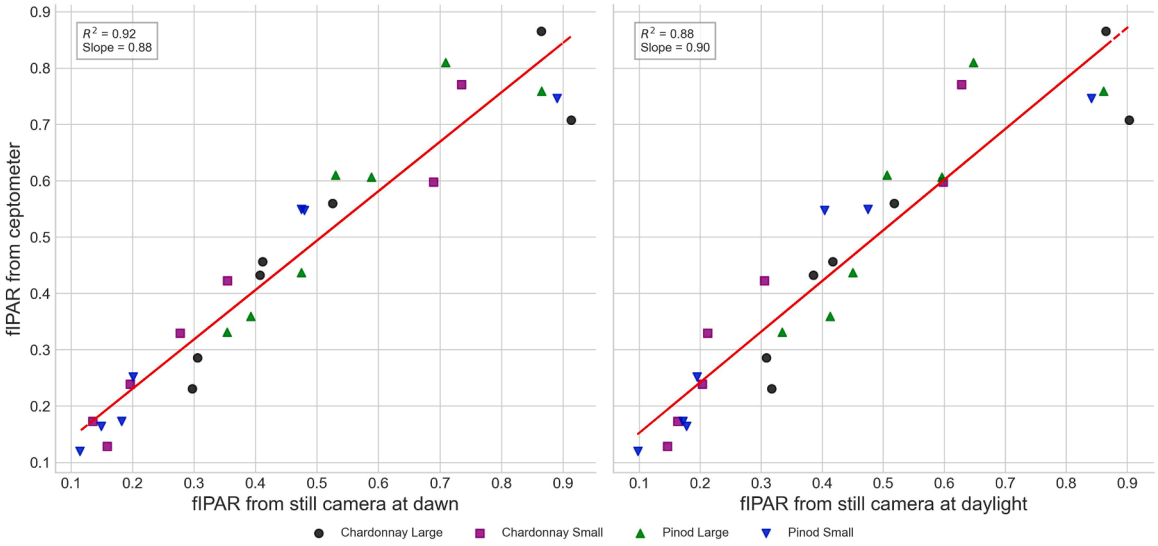

Fig. 10. Regression between fIPAR from diurnal hemispherical imaging and instantaneous ceptometer measurements, comparing dawn and daylight images for four canopies.

(Fig. 10). The performance of the analysis provided sufficient resolution to be able to distinguish between the diurnal patterns represented by all the four examples included in this study. For practical applications in horticulture and irrigation, knowing the exact fIPAR at a specific time is less important. Instead, it's more useful to have a summary of how fIPAR changes throughout the day. This diurnal curve can provide a clearer picture of canopy light interception during daylight hours. The results obtained showed that the hemispherical imaging approach provided similar assessments of the diurnal fIPAR curves for discontinuous canopies as ceptometer readings (Fig. 11), but with a fraction of the labour required to obtain them. The alignment between the instantaneous fIPAR values obtained from ceptometer readings and those from photography was slightly better when the photographic images were taken at dawn.

On the other hand, the instantaneous values shown on the diurnal curves of fIPAR calculated from images acquired at daylight hours were closely correlated with those calculated from images acquired at dawn. In all cases, R^2 was greater than 0.98 (Fig. 12), showing a high repetitiveness of the method, even with different lighting conditions. Nevertheless, the fIPAR values calculated from images corresponding to daylight were slightly lower (3 %) than those of images corresponding to dawn. This difference may be attributed to the effect of sun flares in the images acquired during daylight and its range fits with the estimated maximum effect of sun flares (Fig. 8). It was mostly noticeable around the time the photos were captured, which fits with the commented issue of sun flares affecting pixels at the edge of the canopy. The effect was slightly more pronounced in small canopies.

3.4. Still vs action camera

The average time required to sample a canopy ranged: from 8 to 10 min, using a ceptometer; from 10 to 12 min, using a still camera; and from 1 to 2 min, using an action camera. After downloading the images from the cameras, their processing time in a desktop computer was just few seconds per canopy.

As mentioned earlier, hemispherical imaging allowed us to capture a continuous diurnal pattern of fIPAR. In contrast, the ceptometer only provided discrete fIPAR values at specific times. This limitation was due to the short time window available for measurements. To build a complete diurnal curve using the ceptometer, measurements would need to be repeated at several points throughout the day.

Measurements of fIPAR obtained at the same location, on three consecutive days, made it possible to examine variability between results obtained using a still camera and an action camera. This pointed to their potential for providing a reliable and cost-effective tool for making rapid assessments.

The commercial prices of the devices and accessories required for each approach were $1500, for the ceptometer, $2300, for the still camera with a self-levelling support, and $510, for the action camera. The metrics of variability revealed the interactions between canopy type and temporal variation throughout the day (Fig. 13). The almond canopies, with their larger size and globular-shaped tree crowns, exhibited much less irregularity for the different measurement approaches than the apple and vineyard canopies. In contrast, canopies with a more pronounced edge arrangement, such as those of apple trees and

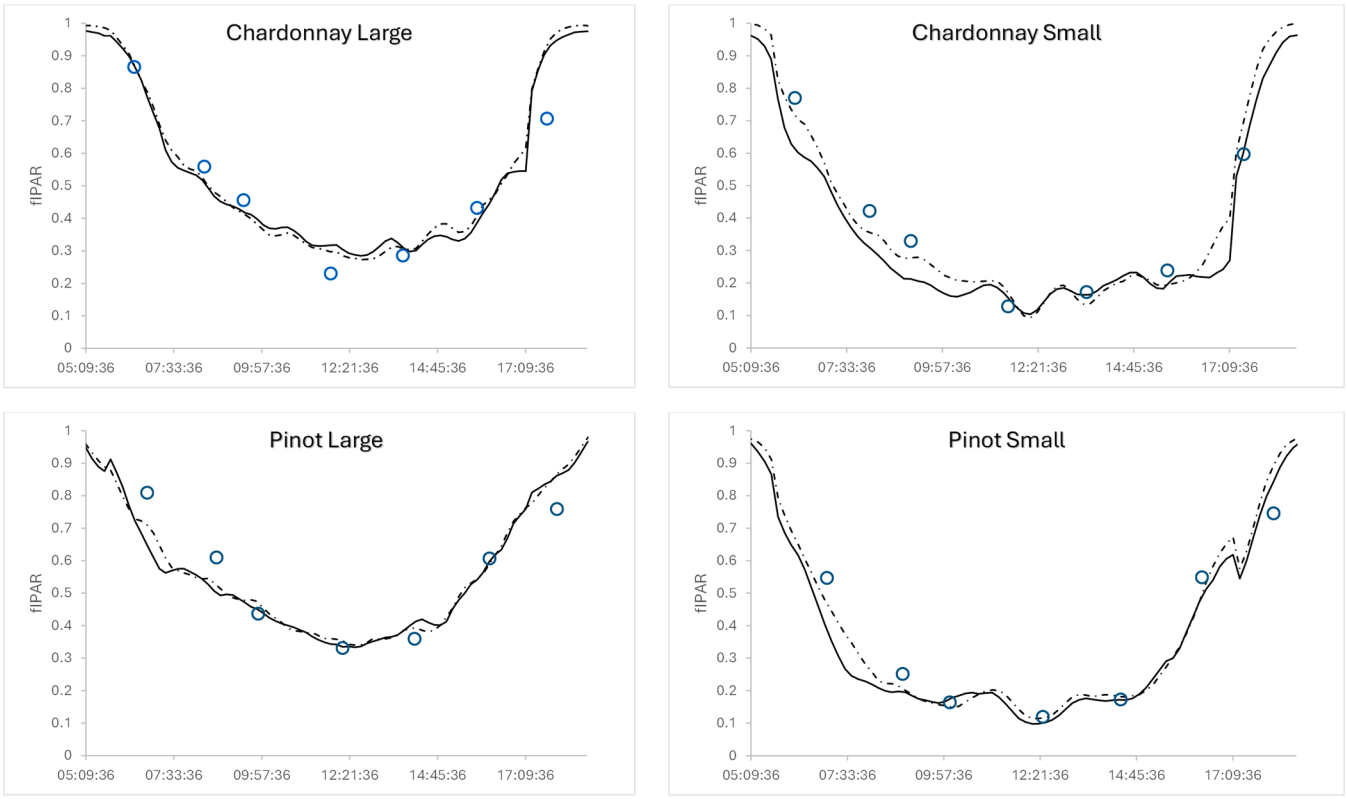

Fig. 11. Diurnal evolution of fIPAR for the four canopies studied, organised by sampling time (daylight represented by the straight line and dawn by the dashed line) vs Ceptometer measurements (shown by dots), and canopy (L: Large, S: Small).

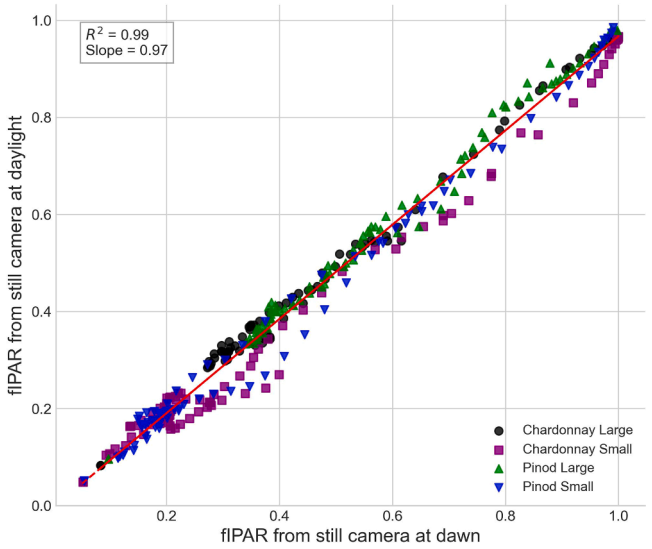

Fig. 12. Correlation between fIPAR sampled at dawn and fIPAR sampled during daylight hours (fIPAR corresponding to a still camera for daylight hours, and fIPAR corresponding to a still camera at dawn).

vineyards, showed diurnal patterns of fIPAR with abrupt changes, particularly at midday. This was probably a result of the pronounced effects that the time of day and solar position had on the interception of beams of sunlight in the case of these narrower canopies. In the case of photographs and videos, the presumed radiation pattern for direct and diffuse components remained constant. However, irregularity in fIPAR from photos and videos occurred from possible changes in the area sampled over the three days of data collection.

Furthermore, values obtained from still and action cameras showed an overall correlation (Fig. 14), supporting their interchangeable use in field data acquisition. Action cameras performed better for tall and near-mature orchards such as the dataset from almond and apple orchards, where the denser canopy and reduced sky fraction above the camera minimized angular biases. In contrast, they tended to overestimate fIPAR in shorter and more open canopies like vineyards, likely due to a wider field of view capturing more the sky against foliage projection when imaging upward.

4. General discussion

The study presents and validates a new DHP methodology which specifically addresses the assessement of a key canopy trait to be used in precision irrigation of tree crops and vineyards, minding the diverse combinations of training systems, tree spacings and crop development that can occur with these crops. In this context, a diurnal fIPAR value considering the radiation intercepted during the whole day would be the ideal parameter.

The DHP approaches proposed in this paper successfully captured diurnal patterns of fIPAR across several different types of canopies. The close alignment between instantaneous fIPAR values obtained using ceptometer readings and the photographic approach underscores the validity of the methodology proposed here, with R^2 values consistently exceeding 0.88. Images obtained at dawn were slightly better than those captured during the day for segmentation and estimating fIPAR. This was likely due to reduced interference from bright sun flares on the images and highlights the tradeoff between optimal ighting conditions and practicity for accomodating the logistics of field sampling. Classic canopy assessments involving the use of hemispherical photography in forests, typically use images obtained at dawn, near sunset, or under overcast sky conditions (Fournier et al., 1996; Fournier and Hall, 2017). This was to avoid problems with sun flares which, with analogic film

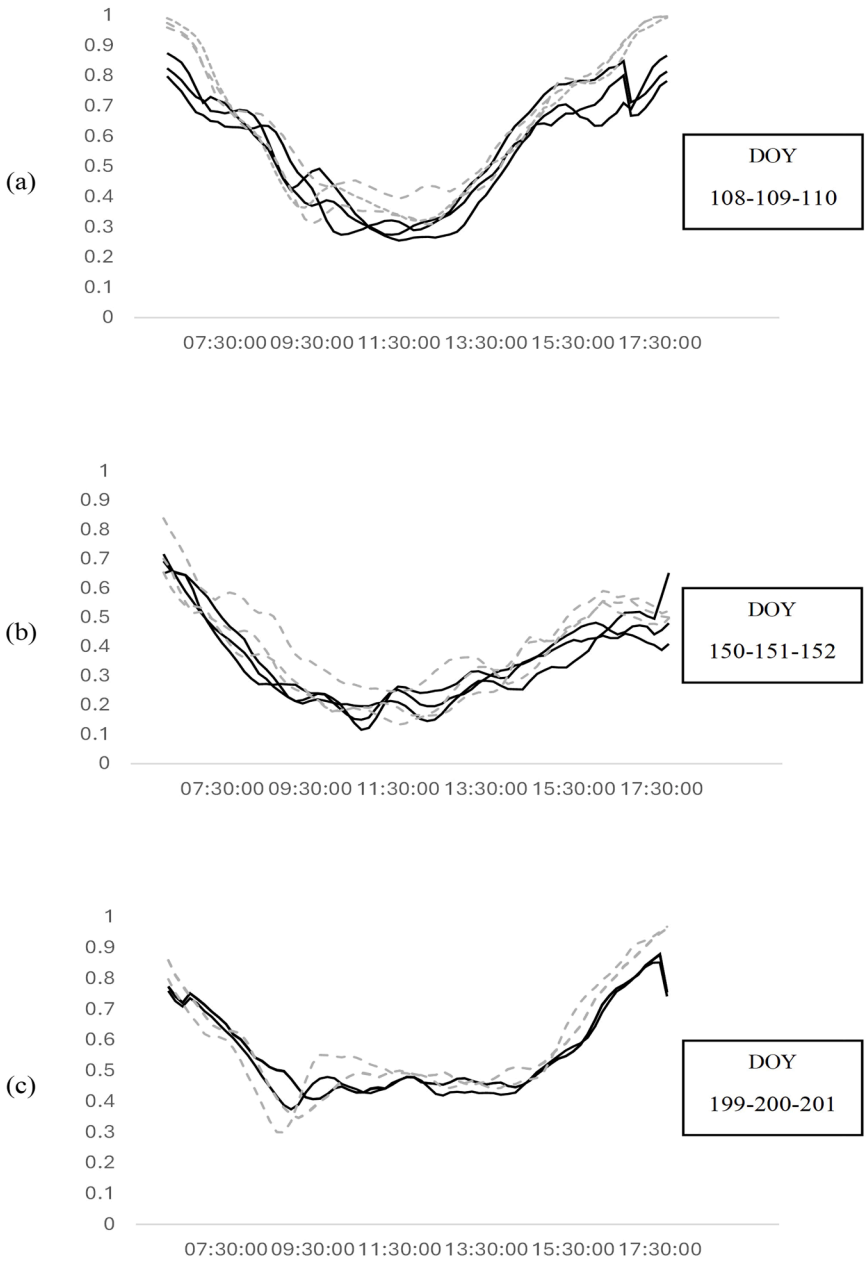

Fig. 13. Diurnal fIPAR curves obtained on three consecutive days using a still camera (continuous line) and an action camera (dashed line) for almond (a), apple (b), and grapevine (c) canopies.

cameras would have ruined the whole photographs. With digital cameras, sun flares only affect a small portion of the image, which can be acceptable as a trade-off against a wider and more practical time window for image sampling. Here we quantified a maximum error that could be caused by sunflares of <3 %, which is acceptable for the assessments of fIPAR in precission irrigation. Furthermore, if necessary for other types of application, the effect of sunflares might be mitigated by integrating advanced flare correction algorithms or supplementary filters during image acquisition.

Ceptometers are currently the main instruments used for assessing fIPAR in horticulture (Anthony et al., 2020; Auzmendi et al., 2011; Cohen et al., 1997; Grossman and DeJong, 1998). However, providing an assessment of representative fIPAR for a whole day with a ceptometer would be very labour intensive and would require clear-sky conditions for the whole diurnal time window. On the other hand, assessments based on the DHP approach proposed here, which uses photos taken using a still camera, required <1 h of work per canopy, without any dependence on the time of day or atmospheric conditions. The labour-saving impact of using a methodology based on photography method is therefore notable and it does not require taking measurements at different times of the day. This photographic approach is also much less sensitive to the time of day and lighting conditions than using a ceptometer. This was shown by the fact that there were only slight differences between diurnal fIPAR curves obtained under two notably different lighting conditions: at dawn and mid-morning. This could have implications for practical assessments of fIPAR in discontinuous canopies since the photographic method can be applied at any time of the day and regardless of the cloud-cover conditions while ceptometer measurements are restricted to a narrow window of daytime and weather conditions.

The comparison of different approaches showed that using action cameras offers an efficient and cost-effective alternative to both ceptometers and still cameras. Still cameras provide high-resolution images, with the camera at a precisely controlled position and orientation,

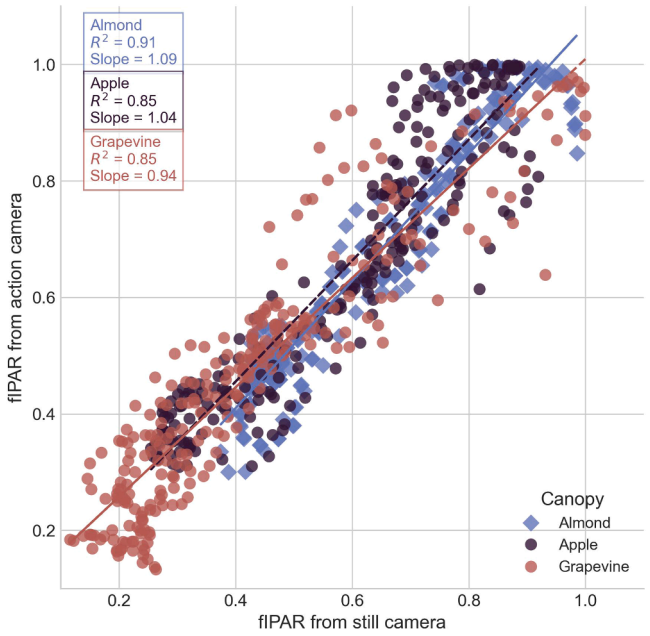

Fig. 14. Correlation between estimations of fIPAR obtained using a still camera and an action camera.

making it suitable for accurate analysis. On the other hand, the ability of action cameras to make continuous recordings in video mode significantly reduces sampling time and enables rapid data acquisition at multiple locations, but with less control on the exact position and orientation of the cameras, thus increasing the risk of sampling errors. The fact that action cameras are cheaper than the other alternatives further emphasize their utility, especially in resource-constrained scenarios or where large-scale applications are required.

Despite the high-level of accuracy and efficiency offered by photographic approaches, certain limitations were noted. Besides the issue with sun flares, there is the challenge of heterogeneous non-natural backgrounds. Variations in anti-hail net properties and in background conditions occasionally required specific adjustments to the segmentation algorithm. The default settings of the algorith are intended for a background ranging from clear blue sky to completely overcast. Color neutral hail nets -the most usual- can acceptably be processed with those settings.

On the other hand, if the nets have colors that cannot be easily distinguished from the canopy, this would require a more adaptable parameterization approach such as using machine learning-based segmentation.

Specialized tools for making canopy measurements have been developed recently, which include devices for estimating LAI and fIPAR. Tools such as the CI-110 Plant Canopy Imager (CID Bio-Science, Washington, USA) provide accurate, non-destructive measurements of canopy structure and light interception. However, beyond economic constraints, there is a methodological need to move beyond single-point measurements and toward characterizing the full diurnal interception curve, which provides a more comprehensive understanding of canopy-light interactions. This approach can improve the robustness of irrigation decision-making. Some of the commercial devices, such as the CI-110, are based on closely related principles to those described here.

Rather than being viewed as alternative methods, they may in fact benefit from the insights and conclusions developed in this study. In addition to advances in devices that permit the direct measurement of PAR-derived parameters (such as intercepted PAR), the option of using simulations based on modelling has been explored (R. S. Johnson and Lakso, 1991; López-Lozano et al., 2011; Mariscal et al., 2000). Such models present various degrees of complexity, ranging from simple models, like that proposed by Oyarzun, Stöckle and Whiting (2007), to more complex ones that incorporate Radiative Transfer Models (RTM) (Guillen-Climent et al., 2012). In operational terms, modelling approaches may complement but not fully replace sensor-based methods, particularly in field conditions where spatial variability and rapid decision-making are key.

5. Conclusions

This manuscript describes and validates a practical approach for improving the representativity of canopy structure assessments of tree crops and vineyards. The approach estimates the diurnal fIPAR curve by tracking the sun path using hemispherical images or video frames. These are captured with an upward-facing camera placed at different positions between the trees to record the canopy from below.

Firstly, this study demonstrates that using a still camera equipped with a fisheye lens and a self-levelling ground support, requiring less than one hour of field work, can offer a rigorous characterization of the pattern of canopy radiation interception. This approach matched the values obtained by measuring fIPAR with a ceptometer along the day. Alternatively, by acquiring the images through short videos with an action camera held on a selfie stick, the required field work is reduced to few minutes. Although the precision can be diminished because of a less controlled positioning and orientation of the camera, the results are still convenient for most applications in horticulture and irrigation management. Moreover, it offers an accessible and scalable option for widespread use.

The proposed methodology proved to offer an operational alternative to using ceptometer-based measurements to assess canopy traits in discontinuous canopies such as those found in vineyards and orchards. Although ceptometers are commonly used for assessing canopy traits at midday, a single measurement taken at that time may not accurately represent the interception pattern for a whole day. To capture a diurnal fIPAR curve using ceptometers, measurements would need to be taken under clear-sky conditions at multiple times during the day. This would not only require suitable weather conditions but also require a significant input of human labour. In contrast, the hemispherical imaging approach described in this study requires only 10 min per assessment and can be applied under a broad range of sky conditions and at any time of the day, making this a practical and cost-saving solution. This methodology is particularly valuable when it is necessary to compare orchards with different training systems. Furthermore, it can be applied beneath crop protection structures, such as anti-hail nets, where obtaining traditional ceptometer measurements may be compromised due to the difficulty of assessing incoming solar radiation below a net.

Declaration of generative AI and AI-assisted technologies in the writing process

During the preparation of this work the author M.I.B used **SCISPACE Paraphraser** to improve the clarity and readability of the text. After using this tool/service, the author reviewed and edited the content as needed and took full responsibility for the content of the publication.

CRediT authorship contribution statement

Mohamed Ibrahim Belaid: Writing – review & editing, Writing – original draft, Visualization, Software, Methodology, Investigation, Formal analysis. **Alexandre Escolà Agustí:** Writing – review & editing, Visualization, Supervision, Conceptualization. **Jaume Casadesús Brugués:** Writing – review & editing, Writing – original draft, Visualization, Validation, Supervision, Software, Methodology, Data curation, Conceptualization.

Declaration of competing interest

The authors declare that they have no known competing financial interests or personal relationships that could have appeared to influence the work reported in this paper.

Acknowledgements

Development and validation of the described method for still cameras was funded by project RTA2010-00007-00-00, from the Spanish Ministry of Agriculture. Its adaptation to action cameras was funded by project ET4DROUGHT, PID2021-127345OR-C31, from the Spanish Agencia Espacial de Investigación. M.I.B was granted a join fellowship from University of Lleida and IRTA.

Data availability

Data will be made available on request.

References

ACCUPAR LP-80 | Leaf Area Index Measurement | METER Environment. (n.d.). Retrieved November 7, 2023, from https://www.metergroup.com/en/meter-environment/products/accupar-lp-80-canopy-interception-par-leaf-area-index.

Allen, R.G., Pereira, L.S., Raes, D., Smith, M., 1998. FAO irrigation and drainage paper No. 56. Rome: Food Agric. Organ. U. N. 56 (97), e156.

Anthony, B., Serra, S., Musacchi, S., 2020. Optimization of light interception, leaf area and yield in "WA38": comparisons among training systems, rootstocks and pruning techniques. Agron. 2020 10 (5), 689. https://doi.org/10.3390/AGRONOMY10050689. *Vol. 10, Page 689*.

Auzmendi, I., Mata, M., Lopez, G., Girona, J., Marsal, J., 2011. Intercepted radiation by apple canopy can be used as a basis for irrigation scheduling. Agric. Water Manag. 98 (5), 886–892. https://doi.org/10.1016/J.AGWAT.2011.01.001.

Baret, F., de Solan, B., Lopez-Lozano, R., Ma, K., Weiss, M., 2010. GAI estimates of row crops from downward looking digital photos taken perpendicular to rows at 57.5° zenith angle: theoretical considerations based on 3D architecture models and application to wheat crops. Agric. Meteorol. 150 (11), 1393–1401. https://doi.org/10.1016/J.AGRFORMET.2010.04.011.

Bellvert, J., Nieto, H., Pelechá, A., Jofre-Čekalović, C., Zazurca, L., Miarnau, X., 2021. Remote sensing energy balance model for the assessment of crop evapotranspiration and water status in an Almond rootstock collection. Front. Plant Sci. 12. https://doi.org/10.3389/FPLS.2021.608967.

Bradski, G., 2000. The opencv library. Dr. Dobb's J.: Softw. Tools Prof. Program. 25 (11), 120–123.

Campbell, G.S., Norman, J.M., 1998. An introduction to environmental biophysics. An Introduction to Environmental Biophysics. Springer, New York. https://doi.org/10.1007/978-1-4612-1626-1.

Campillo, C., Fortes, R., & Del Henar Prieto, M. (2012). *Solar radiation effect on crop production*. www.intechopen.com.

Campillo, C., Prieto, M.H., Daza, C., Moñino, M.J., García, M.I., 2008. Using digital images to characterize canopy coverage and light interception in a processing tomato crop. HortScience 43 (6), 1780–1786. https://doi.org/10.21273/HORTSCI.43.6.1780.

Casadesús, J., Kaya, Y., Bort, J., Nachit, M.M., Araus, J.L., Amor, S., Ferrazzano, G., Maalouf, F., Maccaferri, M., Martos, V., Ouabbou, H., Villegas, D., 2007. Using vegetation indices derived from conventional digital cameras as selection criteria for wheat breeding in water-limited environments. Ann. Appl. Biol. 150 (2), 227–236. https://doi.org/10.1111/J.1744-7348.2007.00116.X;WGROUP:STRING:PUBLICATION.

Casadesús, J., Mata, M., Marsal, J., Girona, J., 2011. Automated irrigation of apple trees based on measurements of light interception by the canopy. Biosyst. Eng. 108 (3), 220–226. https://doi.org/10.1016/J.BIOSYSTEMSENG.2010.12.004.

CI-110 Plant Canopy Imager - CID Bio-Science. (n.d.). Retrieved January 21, 2025, from https://cid-inc.com/plant-science-tools/leaf-area-measurement/ci-110-plant-canopy-imager/.

Cohen, S., Rao, R.S., Cohen, Y., 1997. Canopy transmittance inversion using a line quantum probe for a row crop. Agric. Meteorol. 86 (3–4), 225–234. https://doi.org/10.1016/S0168-1923(96)02426-4.

Díaz, G.M., Lang, M., Kaha, M., 2024. Simple calibration of fisheye lenses for hemispherical photography of the forest canopy. Agric. Meteorol. 352, 110020. https://doi.org/10.1016/J.AGRFORMET.2024.110020.

Drechsler, K., Fulton, A., Kisekka, I., 2022. Crop coefficients and water use of young almond orchards. Irrig. Sci. 40 (3), 379–395. https://doi.org/10.1007/S00271-022-00786-Y/FIGURES/8.

Fournier, R.A., Hall, R.J., 2017. In: Fournier, R.A., Hall, R.J. (Eds.), Hemispherical Photography in Forest Science: Theory, Methods, Applications, Hemispherical Photography in Forest Science: Theory, Methods, Applications, 28. Springer, Netherlands. https://doi.org/10.1007/978-94-024-1098-3.

Fournier, R.A., Landry, R., August, N.M., Fedosejevs, G., Gauthier, R.P., 1996. Modelling light obstruction in three conifer forests using hemispherical photography and fine tree architecture. Agric. Meteorol. 82 (1–4), 47–72. https://doi.org/10.1016/0168-1923(96)02345-3.

Girona, J., del Campo, J., Mata, M., Lopez, G., Marsal, J., 2011. A comparative study of apple and pear tree water consumption measured with two weighing lysimeters. Irrig. Sci. 29 (1), 55–63. https://doi.org/10.1007/S00271-010-0217-5/TABLES/2.

Gower, S.T., Kucharik, C.J., Norman, J.M., 1999. Direct and indirect estimation of Leaf Area Index, fAPAR, and net primary production of terrestrial ecosystems. Remote Sens Environ. 70 (1), 29–51. https://doi.org/10.1016/S0034-4257(99)00056-5.

Green, S., McNaughton, K., Wünsche, J.N., Clothier, B., 2003. Modeling light interception and transpiration of apple tree canopies. Agron J. 95 (6), 1380–1387. https://doi.org/10.2134/AGRONJ2003.1380.

Green, S.R., Greer, D.H., Wünsche, J.N., Caspari, H., 2001. Measurements of light interception and utilization in an apple orchard. Acta Hortic 557, 369–376. https://doi.org/10.17660/ACTAHORTIC.2001.557.49.

Grossman, Y.L., DeJong, T.M., 1998. Training and pruning system effects on vegetative growth potential, light interception, and cropping efficiency in peach trees. J. Am. Soc. Hortic. Sci. 123 (6), 1058–1064. https://doi.org/10.21273/JASHS.123.6.1058.

Guillen-Climent, M.L., Zarco-Tejada, P.J., Berni, J.A.J., North, P.R.J., Villalobos, F.J., 2012. Mapping radiation interception in row-structured orchards using 3D simulation and high-resolution airborne imagery acquired from a UAV. Precis. Agric. 13 (4), 473–500. https://doi.org/10.1007/S11119-012-9263-8.

Hsiao, T.C., 1990. Plant-atmosphere interactions, evapotranspiration, and irrigation scheduling. Acta Hortic. 278, 55–66. https://doi.org/10.17660/ACTAHORTIC.1990.278.3.

Jackson, J.E., Palmer, J.W., 1972. Interception of Light by Model Hedgerow Orchards in Relation to Latitude, Time of Year and Hedgerow Configuration and Orientation. J. Appl. Ecol. 9 (2), 341–357. https://doi.org/10.2307/2402436.

Johnson, R.S., Ayars, J., Trout, T., Mead, R., Phene, C., 2000. Crop coefficients for mature peach trees are well correlated with midday canopy light interception. Acta Hortic. 537, 455–460. https://doi.org/10.17660/ACTAHORTIC.2000.537.53.

Johnson, R.S., & Lakso, A.N. (1991). Approaches to Modeling Light Interception in Orchards.

Johnson, M.V.V., Kiniry, J.R., Burson, B.L., 2010. Ceptometer deployment method affects measurement of fraction of intercepted photosynthetically active radiation. Agron J. 102 (4), 1132–1137. https://doi.org/10.2134/AGRONJ2009.0478.

Jonckheere, I., Fleck, S., Nackaerts, K., Muys, B., Coppin, P., Weiss, M., Baret, F., 2004. Review of methods for in situ leaf area index determination: part I. Theories, sensors and hemispherical photography. Agric Meteorol. 121 (1–2), 19–35. https://doi.org/10.1016/J.AGRFORMET.2003.08.027.

Jones, H., 2013. Radiation. In: Jones, H.G. (Ed.), Plants and Microclimate: A Quantitative Approach to Environmental Plant Physiology, 3rd ed. Cambridge University Press, pp. 9–46. https://doi.org/10.1017/CBO9780511845727.003.

Kotp, Y., & Torki, M. (2023). *Toward flare-free images: a survey*. https://arxiv.org/pdf/2310.14354.

Kotp, Y., Torki, M., 2024. Flare-free vision: empowering uformer with depth insights. In: ICASSP, IEEE International Conference on Acoustics, Speech and Signal Processing - Proceedings, pp. 2565–2569. https://doi.org/10.1109/ICASSP48485.2024.10446006.

Lakso, A.N., 1976. Characterizing apple tree canopies by Fisheye Photography1. HortScience 11 (4), 404–405. https://doi.org/10.21273/HORTSCI.11.4.404.

Lakso, A.N., 2018. Apple. Handbook of Environmental Physiology of Fruit Crops, pp. 3–42.

Lakso, A.N., Intrigliolo, D.S., 2022. Plant-based sensing for irrigation management in the field. Acta Hortic. 1335, 247–262. https://doi.org/10.17660/ACTAHORTIC.2022.1335.30.

Lampinen, B.D., Udompetaikul, V., Browne, G.T., Metcalf, S.G., Stewart, W.L., Contador, L., Negrón, C., Upadhyaya, S.K., 2012. A mobile platform for measuring canopy photosynthetically active radiation interception in orchard systems. HortTechnology 22 (2), 237–244. https://doi.org/10.21273/HORTTECH.22.2.237.

Lampinen, B., Upadhyaya, S., Udompetaikul, V., Browne, G., Roach, J., Metcalf, S., Stewart, W., Contador, L., Negron, C., Gómez, I.P., Beede, B., Debuse, C., Doll, D., Duncan, R., Edstrom, J., Elkins, R., Fichtner, E., Grant, J., Hasey, J., Olson, J., 2014. A second generation mobile platform for assessing midday canopy photosynthetically active radiation interception in orchard systems. Acta Hortic. 1058, 105–112. https://doi.org/10.17660/ACTAHORTIC.2014.1058.10.

López-Lozano, R., Baret, F., Atauri, I.G., de, C., Lebon, E., Tisseyre, B., 2011. 2D approximation of realistic 3D vineyard row canopy representation for light interception (fIPAR) and light intensity distribution on leaves (LIDIL). Eur. J. Agron. 35 (3). https://doi.org/10.1016/j.eja.2011.06.005.

Mariscal, M.J., Orgaz, F., Villalobos, F.J., 2000. Modelling and measurement of radiation interception by olive canopies. Agric. Meteorol. 100 (2–3), 183–197. https://doi.org/10.1016/S0168-1923(99)00137-9.

Marsal, J., Johnson, S., Casadesus, J., Lopez, G., Girona, J., Stöckle, C., 2014. Fraction of canopy intercepted radiation relates differently with crop coefficient depending on the season and the fruit tree species. Agric. Meteorol. 184, 1–11. https://doi.org/10.1016/J.AGRFORMET.2013.08.008.

Massonnet, C., Regnard, J.L., Lauri, P.É., Costes, E., Sinoquet, H., 2008. Contributions of foliage distribution and leaf functions to light interception, transpiration and photosynthetic capacities in two apple cultivars at branch and tree scales. Tree Physiol. 28 (5), 665–678. https://doi.org/10.1093/TREEPHYS/28.5.665.

Masters, G.M., 2004. Renewable and efficient electric power systems. Renew. Effic. Electr. Power Syst. https://doi.org/10.1002/0471668826.

McNaughton, K.G., Green, S.R., Black, T.A., Tynan, B.R., Edwards, W.R.N., 1992. Direct measurement of net radiation and photosynthetically active radiation absorbed by a single tree. Agric Meteorol 62 (1–2), 87–107. https://doi.org/10.1016/0168-1923(92)90007-Q.

Oyarzun, R.A., Stöckle, C.O., Whiting, M.D., 2007. A simple approach to modeling radiation interception by fruit-tree orchards. Agric. Meteorol. 142 (1), 12–24. https://doi.org/10.1016/J.AGRFORMET.2006.10.004.

Palmer, J.W., 1977. Diurnal light interception and a computer model of light interception by Hedgerow Apple Orchards. J. Appl. Ecol. 14 (2), 601. https://doi.org/10.2307/2402570.

Quintanilla-Albornoz, M., Miarnau, X., Pelechá, A., Casadesús, J., García-Tejera, O., Bellvert, J., 2023. Evaluation of transpiration in different almond production systems with two-source energy balance models from UAV thermal and multispectral imagery. Irrig. Sci. 1, 1–21. https://doi.org/10.1007/S00271-023-00888-1/FIGURES/11.

Sangjan, W., Sankaran, S., 2021. Phenotyping architecture traits of tree species using remote sensing techniques. Trans. ASABE 64 (5), 1611–1624. https://doi.org/10.13031/TRANS.14419.

Scalisi, A., O'Connell, M.G., Stefanelli, D., Zhou, S., Pitt, T., Graetz, D., Dodds, K., Han, L., De Bei, R., Stanley, J., Breen, K., Goodwin, I., 2024. Narrow orchard systems for pome and stone fruit—A review. Sci. Hortic. 338, 113815. https://doi.org/10.1016/J.SCIENTA.2024.113815.

Steduto, P., Hsiao, T.C., Fereres, E., Raes, D., 2012. Crop Yield Response to Water, 1028. fao, Rome.

Tustin, D.S., Breen, K.C., Van Hooijdonk, B.M., 2022. Light utilisation, leaf canopy properties and fruiting responses of narrow-row, planar cordon apple orchard planting systems—A study of the productivity of apple. Sci. Hortic. 294, 110778.

Weiss, M., Baret, F., Smith, G.J., Jonckheere, I., Coppin, P., 2004. Review of methods for in situ leaf area index (LAI) determination part II. Estimation of LAI, errors and sampling. Agric. Meteorol. 121 (1–2), 37–53. https://doi.org/10.1016/j.agrformet.2003.08.001.

Wünsche, J.N., Lakso, A.N., 2000. The relationship between leaf area and light interception by spur and extension shoot leaves and apple orchard productivity. HortScience 35 (7), 1202–1206. https://doi.org/10.21273/HORTSCI.35.7.1202.

Wünsche, J.N., Lakso, A.N., Robinson, T.L., 1995. Comparison of four methods for estimating total light interception by apple trees of varying forms. HortScience 30 (2), 272–276. https://doi.org/10.21273/HORTSCI.30.2.272.

Wünsche, J.N., Lakso, A.N., Robinson, T.L., Lenz, F., Denning, S.S., 1996. The bases of productivity in Apple production systems: the role of light interception by different shoot types. J. Am. Soc. Hortic. Sci. 121 (5), 886–893. https://doi.org/10.21273/JASHS.121.5.886.

Zarate-Valdez, J.L., Metcalf, S., Stewart, W., Ustin, S.L., Lampinen, B., 2015a. Estimating light interception in tree crops with digital images of canopy shadow. Precis. Agric. 16 (4), 425–440. https://doi.org/10.1007/S11119-015-9387-8/FIGURES/8.

Zarate-Valdez, J.L., Muhammad, S., Saa, S., Lampinen, B.D., Brown, P.H., 2015b. Light interception, leaf nitrogen and yield prediction in almonds: a case study. Eur. J. Agron. 66, 1–7. https://doi.org/10.1016/J.EJA.2015.02.004.

Zarate-Valdez, J.L., Whiting, M.L., Lampinen, B.D., Metcalf, S., Ustin, S.L., Brown, P.H., 2012. Prediction of leaf area index in almonds by vegetation indexes. Comput. Electron. Agric. 85, 24–32. https://doi.org/10.1016/J.COMPAG.2012.03.009.

Zhang, J., Luo, R., Scharf, P., Whiting, M., Zhang, Q., 2012. Canopy architecture affects light interception in sweet cherry your. In: *American Society of Agricultural and Biological Engineers Annual International Meeting 2012, ASABE 2012, 2*, 1-. https://doi.org/10.13031/2013.41789.

Zhang, J., Whiting, M.D., Zhang, Q., 2015. Diurnal pattern in canopy light interception for tree fruit orchard trained to an upright fruiting offshoots (UFO) architecture. Biosyst. Eng. 129, 1–10. https://doi.org/10.1016/J.BIOSYSTEMSENG.2014.09.005.